

Article

Stereoselectivity in Butadiene Polymerization Promoted by Using Ziegler–Natta Catalysts Based on (Anilidomethyl)pyridine Group (IV) Complexes

Stefano Milione * and Stefania Pragliola 

Department of Chemistry, University of Salerno, Via Giovanni Paolo II, 84084 Fisciano, Salerno, Italy; spragliola@unisa.it

* Correspondence: smilione@unisa.it

Abstract: The stereoselective polymerization of conjugated dienes promoted by using transition metal complexes has attracted much interest in both industrial and academic environments for the relevance of polydienes as synthetic rubbers and for the challenging reaction mechanisms. Among the different transition metal complexes, those based on group IV have been demonstrated to be versatile and efficient catalysts. Titanium complexes are generally more active than zirconium complexes. A rare exception to this trend is represented by a series of Zr(IV) complexes supported by (anilidomethyl)pyridine ligands that, after activation by using Al(*i*Bu₂H)/MAO, were found to be highly active affording exclusively *cis*-1,4-polybutadiene. To rationalize this unexpected trend and to obtain more insights into the parameters that control the reactivity of group IV complexes, a theoretical investigation of the entire polymerization mechanism, employing density functional methods, was undertaken. In the framework of the widely accepted polymerization scheme, the different intermediates featuring h⁴ (both *cis* and *trans*) coordination of the monomer and h¹ or h³ (*syn* or *anti*)allyl coordination of the growing chain were scrutinized. Subsequently, the effects of the metal center on the free-energy profiles of the elementary steps involved in the reaction were examined. The results presented herein aim to achieve a better knowledge of the influence of the metal on the polymerization rates and on the stereoselectivity of the reaction.

Keywords: diene polymerization; Ziegler–Natta catalyst; DFT calculation

Citation: Milione, S.; Pragliola, S. Stereoselectivity in Butadiene Polymerization Promoted by Using Ziegler–Natta Catalysts Based on (Anilidomethyl)pyridine Group (IV) Complexes. *Symmetry* **2024**, *16*, 18. <https://doi.org/10.3390/sym16010018>

Academic Editor: György Keglevich

Received: 30 November 2023

Revised: 14 December 2023

Accepted: 19 December 2023

Published: 22 December 2023



Copyright: © 2023 by the authors. Licensee MDPI, Basel, Switzerland. This article is an open access article distributed under the terms and conditions of the Creative Commons Attribution (CC BY) license (<https://creativecommons.org/licenses/by/4.0/>).

1. Introduction

One of the everlasting challenges in polymer chemistry is synthesizing new materials with targeted properties. This can be achieved accurately by controlling the microstructures of the polymer chains. 1,3-butadiene is usually polymerized by using Ziegler–Natta catalytic systems affording polymers with the designed properties [1–6]. Depending on the chosen catalyst, different stereoregular polybutadienes, *iso*-1,2, *syndio*-1,2, *cis*-1,4, and *trans*-1,4-polybutadiene, can be prepared, each with peculiar features [7–16]. Of all of them, *cis*-1,4-polybutadiene has gained increasing attention from the industrial world due to its excellent properties, so it is true that, as regards the industrial production of synthetic rubbers, it is second in the world, surpassed only by styrene–butadiene rubber. The two forms of *cis*-1,4-polybutadiene currently marketed are low *cis*-1,4-polybutadiene containing approximately 40% 1,4-*cis* repeating units and high *cis*-1,4-polybutadiene, which has a content of 1,4-*cis* between 92 and 98% [17]. As for high *cis*-1,4-polybutadiene, its highly linear molecular structure and regularity mean that it exhibits an excellent elasticity, a high mechanical strength, a low heat accumulation, and a strong resistance to abrasion and fatigue stress, which make it particularly suitable as a tire manufacturing material [18,19]. Catalytic systems based on titanium halides and aluminum alkyls were the first to be used in *cis*-1,4-polybutadiene industrial production [6]. Subsequently, thanks to the in-depth theoretical and experimental studies of many researchers from both the

academic and industrial worlds, other systems with higher activity and stereospecificity were developed. It was discovered that catalytic systems made up of transition metal complexes like chromium, iron, cobalt, and nickel with phosphorus and nitrogen ligands and methylaluminoxane (MAO) are highly active in 1,3-butadiene polymerization. Moreover, the *cis*-1,4 microstructure can be optimized by varying both ligands and metals [20–27]. Neodymium-based catalytic systems also show outstanding performance in the *cis*-1,4 polymerization of 1,3-butadiene. They give linear polymers with a high content of *cis*-1,4 units in aliphatic solvents, while show worse performance in aromatic solvents [28,29]. Currently, catalysts based on titanium, neodymium, nickel, and cobalt compounds showing excellent performances and reaching a *cis* specificity up than 90% are employed for high *cis*-1,4-polybutadiene industrial production. Due to their poor activity for the conjugated diene polymerization, zirconium catalysts have been less studied. However, in 2011, a study on 1,3-butadiene polymerization with catalytic systems consisting of both Ti(IV) and Zr(IV) (anilidomethyl)pyridine complexes and Al(*i*Bu₂H)/MAO was reported in the literature [30]. Unexpectedly, zirconium-based catalysts showed higher activity and stereospecificity with respect to the titanium homologous providing polymers with a content of 1,4 *cis* up 99.9% [30]. To the best of our knowledge, this is the only case reported in the literature of zirconium-based catalytic systems providing solely *cis*-1,4-poly(butadiene) with quite high activities. To rationalize the unexpected experimental results indicating better performances of Zr-based catalysts compared to Ti-based ones, in this work, a theoretical study concerning the entire mechanism controlling the 1,3-butadiene polymerization was performed. By applying established density functional methods (DFT), an attempt was made to thoroughly understand the origin of the high stereospecificity of 1,3-butadiene polymerization under the action of catalytic systems based on (anilidomethyl)pyridine Zr(IV) complexes. It is worth underlining that designing and producing new and more efficient industrial catalysts to produce high *cis*-polybutadiene is still challenging, and close attention is currently paid to both experimental and theoretical studies on this matter. In particular, the development of theoretical quantum chemical methods allows for clarification of the mechanistic aspects involved in the ion-coordination polymerization of dienes as well as for the offering of new solutions in catalysis.

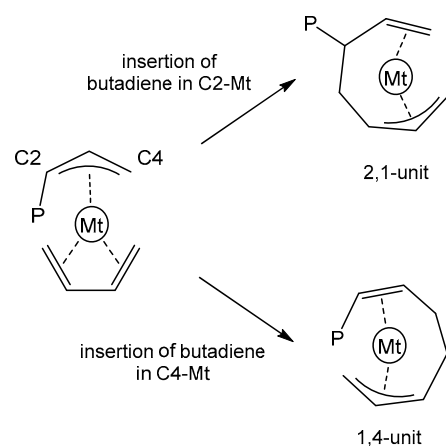
2. Materials and Methods

Computational details. All DFT calculations were performed at the GGA level with the Gaussian 09 set of programs [31], using the BP86 functional of Becke and Perdew [32,33]. The electronic configuration of the molecular systems was described with the standard split valence basis set with a polarization function of Ahlrichs and co-workers for H, C, and N (SVP keyword in Gaussian) [34]. For Ti and Zr, we used the LanL2DZ basis set with associate effective core potentials [35]. Geometry optimizations were performed without symmetry constraints, and all the obtained structures were validated as minima or transition states by using the vibrational frequency calculations. These frequencies were used to calculate unscaled zero-point energies (ZPEs) as well as thermal corrections and entropy effects at 298 K and 1 atm by using the standard statistical mechanics relationships for an ideal gas. Energies were obtained via single-point calculations on the BP86-optimized geometries using the M06 functional [36]. In these single-point energy calculations, H, C, and N were described by using the TZVP basis set, whereas for the metals (Ti or Zr), the LanL2DZ basis set was employed. On top of the M06/TZVP~LanL2DZ//BP86-D3/SVP~LanL2DZ energies, we added the ZPE thermal and entropy corrections obtained at the BP86/SVP~LanL2DZ level. The buried volume calculations were performed with the SambVca 2.1 package, a software free of charge developed by Cavallo et al [37]. The radius of the sphere around the metal center was set to 3.5 Å, while for the atoms, we adopted the Bondi radii scaled by 1.17, and a mesh of 0.1 Å was used to scan the sphere for buried voxels. The coordinates of all the optimized structures as well as their main energetic features are available on request.

3. Results and Discussion

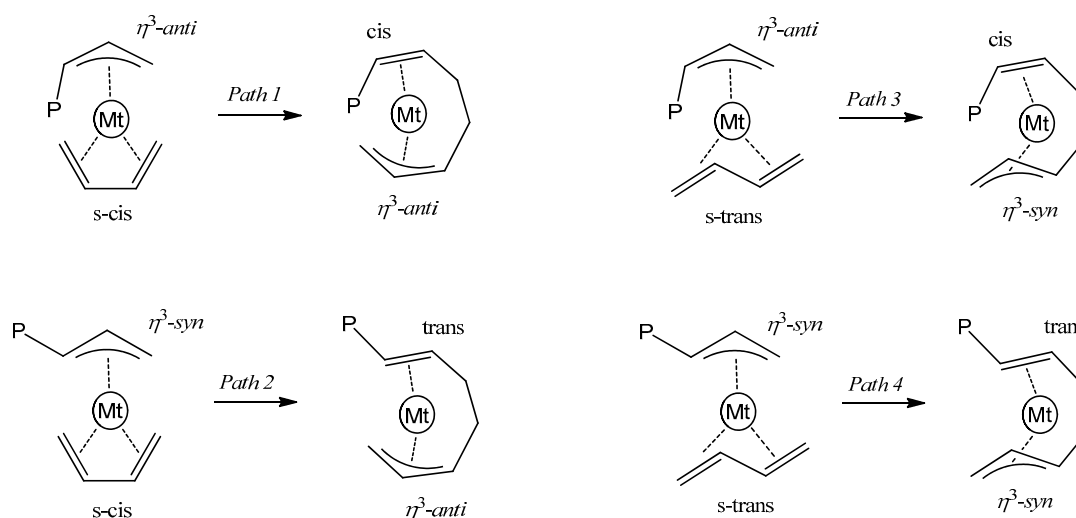
3.1. General Considerations

The generally accepted mechanism for 1,3-butadiene polymerization assumes that, during the propagation stage, the growing polymer chain is bounded to the metal center through a terminal allyl group in a η^1 or η^3 coordination mode, with a *syn*- or *anti*-configuration [38–48]. 1,3-butadiene is coordinated in a monodentate (η^2) or bidentate mode (η^4) and can display either a *s-cis* or a *s-trans* conformation. Depending on the insertion of butadiene involving the terminal C4 or internal C2 carbon atom of the allyl group, 1,4- or 2,1-insertion occurs (Scheme 1). In this work, the path for 2,1-insertion was not investigated as the (anilidomethyl)pyridine–zirconium catalyst produces polymers featuring exclusively 1,4-enchainment butadiene units. The titanium catalyst affords polymers with a content of 2,1-units lower than 10% [30].



Scheme 1. 1,4- vs. 2,1-insertion.

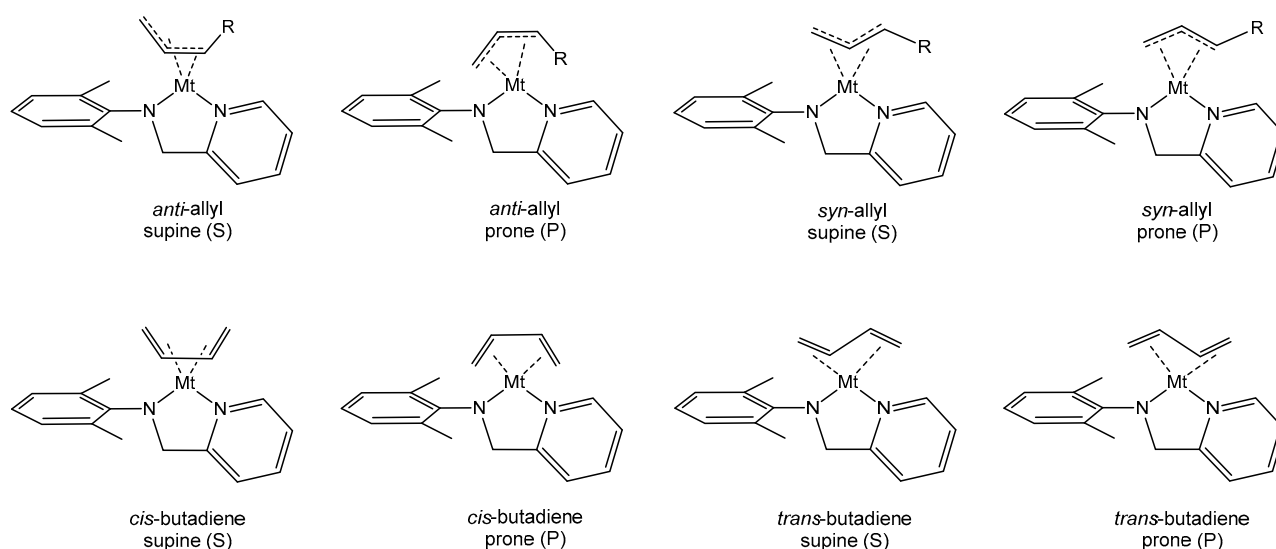
The stereochemistry of the insertion reaction, i.e., the formation of the 1,4-*cis* or 1,4-*trans* repeating unit depends on the configuration of the allyl terminal group. The insertion step involving the allyl group with the *anti*-configuration leads to a 1,4-*cis* repeating unit, whereas the insertion step involving the allyl group with the *syn*-configuration leads to a 1,4-*trans* repeating unit [38–48]. Depending on the configuration of the allyl group and butadiene, the insertion step can occur through the four competitive paths depicted in Scheme 2.



Scheme 2. Competitive paths for 1,4-insertion.

The conformation of the allyl group is in turn determined by the configuration of the incoming monomer: the insertion step involving the monomer coordinated to the metal center in a *s-cis* or *s-trans* configuration produces an *anti*- or a *syn*-allyl terminal group, respectively. Definitively, the formation of 1,4-*cis*-polybutadiene (or 1,4-*trans*-polybutadiene) is realized when the insertion step exclusively occurs through *path 1* (or *path 4*). *Path 2* and *path 3* lead to a change in the configuration of the repeating unit.

The species investigated in this study will be indicated as follows: 1_{Mt} for the butadiene–allyl complex, TS_{1-2Mt} for the transition state for the monomer insertion, and 2_{Mt} for the insertion product (Mt = Ti or Zr). To calculate the structures and the energies of $1_{Mt-2_{Mt}}$, the mutual arrangement of the butadiene and the allyl groups have to be taken into account. In other words, in each intermediate or transition state, the concavity of the allyl and the *s-cis* or *s-trans* butadiene can be oriented in different ways to each other and with respect to the (anilidomethyl)pyridine ligand. We will indicate as supine (S) the allyl group, the *s-cis* or the *s-trans* butadiene orienting the concavity toward the ligand and we will indicate as prone (P) the allyl group, the *s-cis* or the *s-trans* butadiene orienting the concavity in the opposite direction. These different modes of coordination are displayed in Scheme 3.



Scheme 3. Coordination modes for butadiene and butenyl groups.

3.2. Model of the Active Species

The active species involved in the Ziegler–Natta polymerization is a cationic–alkyl complex that originates from the reaction of the precatalyst with MAO or other activation agents. In the activation reaction, the precatalyst is first converted in an alkyl derivative, then, it undergoes an alkyl abstraction reaction to form a cationic alkyl derivative that, after coordination of the monomer, can start polymerization.

The alkylation of the (anilidomethyl)pyridine group precatalysts should lead to a trialkyl derivative of the general formula $(NN)MtR_3$. In a first instance, we considered the monovalent cation that originates from the abstraction of one alkyl group from the tri-alkyl derivative: $(NN)MtRR'(CH_2=CHCH=CH_2)^+$. In this species, R represents the growing polymer chain, and R' is a second alkyl group bound to the metal atom. In our calculation, the growing polymer chain was modeled with the butenyl group, and the second alkyl group was modeled with a methyl group. Using this model for the active species, the calculations were inconclusive and not useful for explaining the experimental results.

So, we turned to consider as active species the divalent cation that originates from the abstraction of two alkyl groups from the tri-alkyl derivative: $(NN)MtR(CH_2=CHCH=CH_2)^{2+}$. The results described herein were obtained using this model. Its steric map indicating the encumbering of the ligand in the proximity of the active site is reported in Figure 1 [37].

The metal atom is at the center of the sphere, and the complex is oriented with the ligand lying between the northern and the southern hemispheres. The two alkyl substituents of the anilido group producing the two bulges in the north–west and south–west quadrants encumber the western hemisphere, and the percent of buried volume is 26.8%. The eastern hemisphere is substantially more open, and the percent of buried volume is 12.0%. In our model, we assumed that the growing polymer chain is bound to the metal center turning the bulky alkyl tail toward the less-crowded area, i.e., toward the pyridine substituent.

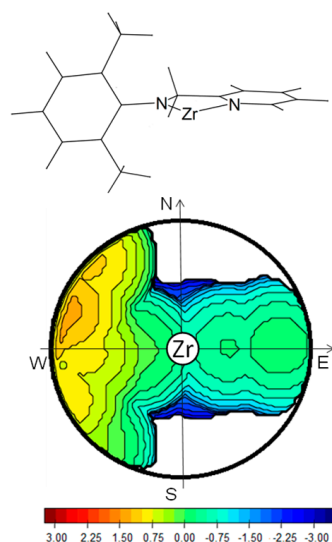


Figure 1. Steric encumber determined by using (anilidomethyl)pyridine ligand. The isocontour curves are given in Å. (% V_{bur} = 38.8).

3.3. Polymerization Paths Promoted by Using the Zirconium-Based Catalyst

Sixteen isomers are expected for the butadiene– π complex 1_{Zr} , and their energies are reported in Table 1. The most stable one features the butenyl group η^3 -coordinated to the metal center with the *anti*-conformation and the butadiene coordinated in a η^4 -bidentate mode with the *trans* conformation ($1_{\text{Zr_anti-S/trans-P}}$). The differences in free energies spread in the range from 0.0 to 9.7 kcal/mol cause the different steric interactions among the butenyl group, the monomer, and the (anilidomethyl)pyridine ligand. The optimized structures of the isomer with the *anti*-butenyl group and η^4 -*cis*-butadiene ($1_{\text{Zr_anti-S/cis-S}}$) and the isomer with the *syn*-butenyl group and η^4 -*trans*-butadiene ($1_{\text{Zr_syn-P/trans-S}}$) are reported in Figure 2. The butenyl group is coordinated in a symmetrical mode: the carbon atom C1 is at a longer distance from zirconium with respect to the carbon atom C3. Butadiene is coordinated with a comparable bond distance for the two non-terminal carbon atoms.

Starting from the isomers of 1_{Zr} , the insertion of the η^4 -coordinated butadiene into the Zr–butenyl bond occurs passing through the transition state $TS_{1-2\text{Zr}}$. All the possible structures were located, and the corresponding activation free energies are reported in Table 1. A close inspection of the geometries reveals that their energies are related to the mutual positioning of the zirconium atom, terminal reactive C1 of the butenyl group, and butadiene’s double bond. When these atoms lay in a quasi-planar arrangement, an energetically favorable transition is realized. Those isomers that present a non-planar arrangement of these atoms are energetically unfavorable. In Figure 2, the optimized structure of the transition states for the *cis*-butadiene insertion on the isomer with the *anti*-butenyl group and for the *trans*-butadiene insertion on the isomer with the *syn*-butenyl group are reported. The distances of the emerging C–C bond are 2.17 Å and 2.08 Å, respectively, and the bond distances of the other groups resemble those of the starting reagents.

Following the intrinsic reaction coordinate, the transition states $TS_{1-2\text{Zr}}$ lead to the products of the reaction 2_{Zr} in which the monomer is inserted, and a new allyl terminal

group is formed. The reactions are exergonic in all cases. The structures of the two products emerging from the transition state structures reported in Figure 2 are included in the same figure.

Table 1. Calculated Gibbs free energies for all the species involved in the 1,4-butadiene insertion in the Zr–butenyl bond (see Supplementary Materials).

	Path 1			Path 3		
	1_{Zr}	TS_{1-2Zr}	2_{Zr}	1_{Zr}	TS_{1-2Zr}	2_{Zr}
<i>anti</i> -S/ <i>cis</i> -S	4.4	10.0	−6.1	<i>anti</i> -S/ <i>trans</i> -P	0.0	21.4
<i>anti</i> -S/ <i>cis</i> -P	5.2	22.9	−5.6	<i>anti</i> -S/ <i>trans</i> -S	1.2	11.0
<i>anti</i> -P/ <i>cis</i> -S	9.7	12.3	−3.9	<i>anti</i> -P/ <i>trans</i> -P	4.5	23.0
<i>anti</i> -P/ <i>cis</i> -P	6.6	25.0	−4.0	<i>anti</i> -P/ <i>trans</i> -S	4.3	16.3
	Path 2			Path 4		
	1_{Zr}	TS_{1-2Zr}	2_{Zr}	1_{Zr}	TS_{1-2Zr}	2_{Zr}
<i>syn</i> -S/ <i>cis</i> -S	6.2	11.0	−7.2	<i>syn</i> -S/ <i>trans</i> -P	2.5	22.6
<i>syn</i> -S/ <i>cis</i> -P	5.5	21.1	−5.8	<i>syn</i> -S/ <i>trans</i> -S	2.8	13.7
<i>syn</i> -P/ <i>cis</i> -S	5.8	8.4	−7.4	<i>syn</i> -P/ <i>trans</i> -P	4.8	20.9
<i>syn</i> -P/ <i>cis</i> -P	5.3	21.9	−5.3	<i>syn</i> -P/ <i>trans</i> -S	5.1	12.9

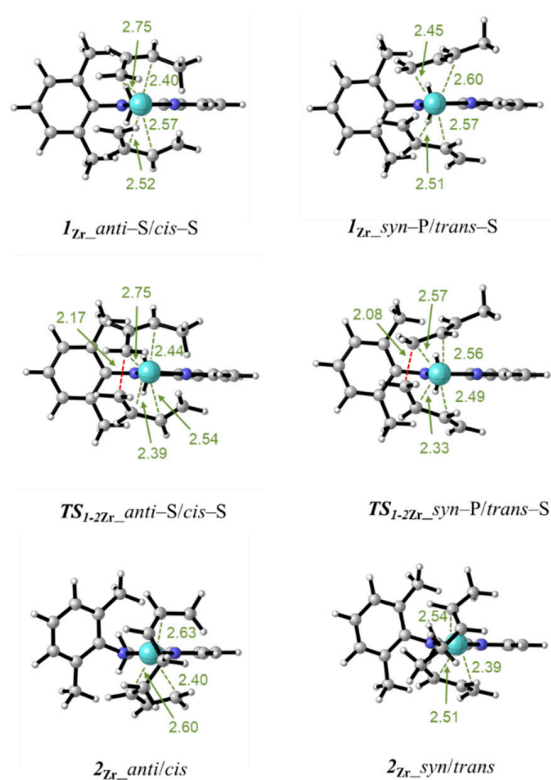


Figure 2. Minimum energy structures for the butadiene– π complex 1_{Zr} , the transition state TS_{1-2Zr} , and the insertion product 2_{Zr} . The isomers having the *anti*-butenyl group and the *cis*-coordinated butadiene (left column) and having the *syn*-butenyl group and the *trans*-coordinated butadiene (right column) are displayed. The distances are given in Angstrom.

To discuss the *cis/trans* selectivity, we compared the Gibbs free-energy profiles of the four possible paths discussed in Scheme 2. Each path involves four different isomers, and we focused exclusively on that isomer to which the lowest activation barrier corresponds. The Gibbs free-energy profiles comparing the four paths are given in Figure 3. The most feasible paths are *path 1* and *path 2*, and both start from the isomers with the butadiene coordinated in η^4 -*cis*-mode and lead to the insertion products featuring the growing polymer

chain coordinated in the *anti*-mode (*cis*-butadiene route). The required activation barriers are about 2 kcal/mol lower than those required for the *trans*-butadiene insertion routes. Regarding the *cis*-butadiene insertion into the *syn*- and *anti*-isomers, it results that the *syn*-isomer is slightly more reactive than the *anti*-isomer, and the difference in the insertion barriers is 1.6 kcal/mol. Based on kinetic considerations, the most-favored product is product $2_{Zr_anti/trans}$. To deepen the investigation, we calculated the energy required to lengthen the polymer chain by another butadiene unit in the following propagation cycle. The corresponding Gibbs free-energy profile is reported in Figure 4. Starting from $2_{Zr_anti/trans}$, the monomer coordination leads to the isomer $3_{Zr_anti-S/cis-S}$ in which the butadiene is *cis*-coordinated or leads to isomer $3_{Zr_anti-S/trans-S}$ in which the butadiene is *trans*-coordinated. The process is exergonic for both cases. The subsequent insertion is more favored for the *cis*-coordinated butadiene, and the difference between the Gibbs free energies of the two transition states ($\Delta\Delta G$) is 2.6 kcal/mol. The kinetic product of insertion $4_{Zr_anti/cis}$ still features the polymer chain coordinated in the *anti*-manner and can initiate a catalytic cycle identical to the previous one. The succession of these catalytic cycles leads to the formation of a polymer chain in which the monomer is linked exclusively in a 1,4-*cis* mode.

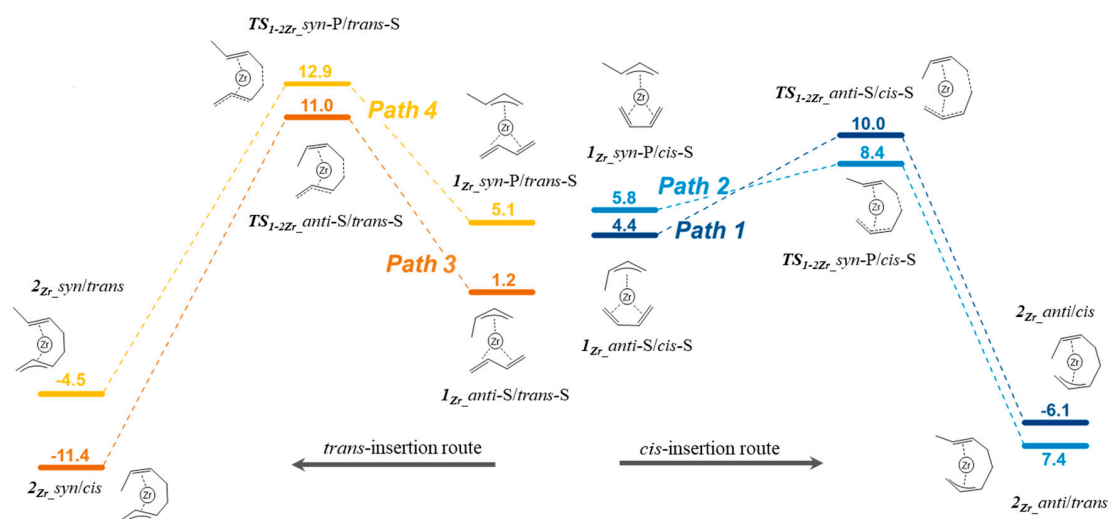


Figure 3. Gibbs free-energy profile for butadiene insertion in the Zr-butanyl bond.

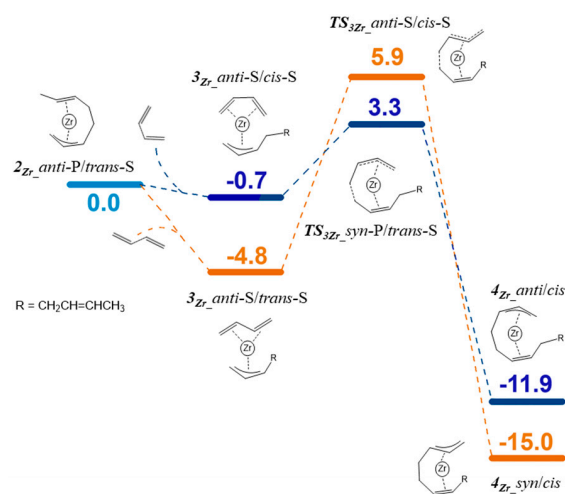
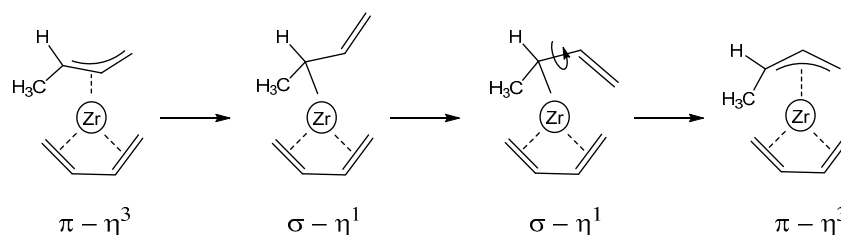


Figure 4. Gibbs free-energy profile for the second butadiene insertion in the Zr-butanyl bond.

It is worth noting that the regioselectivity of the butadiene insertion is affected by the *anti*-*syn* isomerization of the growing polybutadienyl chain. As matter of fact, the

interconversion of the butenyl terminal group in $2_{Zr_anti-P/trans-S}$ from the *anti*-form to the *syn*-form opens the way to the concatenation of the butadiene in the 1,4-*trans* mode. The most-accepted mechanism for this isomerization is shown in Scheme 4. In a first step, the butenyl group bounded to the metal center changes its coordination mode from the $\pi-\eta^3$ to the $\sigma-\eta^1$, and the rotation around the C2–C3 single bond of the vinyl group follows, and, at the end, the butenyl group returns to the $\pi-\eta^3$ coordination mode. Starting from $1_{Zr_anti-S/cis-S}$, we searched for the isomer featuring the polymer chain bound to the metal with the $\eta^1-\sigma$ coordination mode, and it was successfully located at 10.0 kcal/mol higher than the starting isomer. Its energy is higher than all the isomers and transition states reported in Figure 3, and this means that it is thermodynamically and kinetically inaccessible. We can state that the *syn-anti* isomerization is not a competitive path for the 1,4-butadiene insertion in the growing polymer chain.



Scheme 4. *Syn-anti* isomerization.

3.4. Polymerization Paths Promoted by Using the Titanium-Based Catalyst

The energies of all the isomers and transition states involved in the competitive reactions for the butadiene insertion in the Ti–butenyl bond are reported in Table 2. The energies of all the isomers of the butadiene– π complex (1_{Ti}) are comprised between 0.0 and 8.6 kcal/mol. In this case, the most stable isomer features the *syn*-terminal butenyl group and the *trans*-coordinated butadiene ($1_{Ti_syn-S/trans-S}$). For comparative purposes, the optimized structures of the isomer with the *anti*-butenyl group and η^4 -*cis*-butadiene ($1_{Ti_anti-S/cis-S}$) and the isomer with the *syn*-butenyl group and η^4 -*trans*-butadiene ($1_{Ti_syn-P/trans-S}$) are displayed in Figure 5. It can be seen that, in accordance with the lower ionic radius of the titanium atom, the Ti–C bond distances are shorter than the analogue Zr–C bond distances. This causes a crowding in the coordination and a greater repulsion between the coordinated monomer and the growing polymer chain. As a result, the coordination of the butadiene is highly asymmetric and occurs, in some cases, in a monodentate (η^2) rather than bidentate mode (η^4), (see, for example, the structure of the isomer $1_{Ti_anti-S/cis-S}$ in Figure 5).

Table 2. Calculated Gibbs free energies for all the species involved in the 1,4-butadiene insertion in the Ti–butenyl bond (see Supplementary Materials).

	Path 1			Path 3			
	1_{Ti}	TS_{1-2Ti}	2_{Ti}	1_{Ti}	TS_{1-2Ti}	2_{Ti}	
<i>anti-S/cis-S</i>	3.2	5.4	−12.4	<i>anti-S/trans-P</i>	0.2	15.4	−12.1
<i>anti-S/cis-P</i>	4.8	15.5	−11.1	<i>anti-S/trans-S</i>	0.8	8.0	−13.2
<i>anti-P/cis-S</i>	8.6	8.7	−11.7	<i>anti-P/trans-P</i>	3.5	15.9	−5.2
<i>anti-P/cis-P</i>	6.1	18.6	−4.3	<i>anti-P/trans-S</i>	3.2	8.6	−8.9
	Path 2			Path 4			
	1_{Ti}	TS_{1-2Ti}	2_{Ti}	1_{Ti}	TS_{1-2Ti}	2_{Ti}	
<i>syn-S/cis-S</i>	5.2	-	−13.0	<i>syn-S/trans-P</i>	1.0	15.8	−9.7
<i>syn-S/cis-P</i>	4.2	14.2	−3.7	<i>syn-S/trans-S</i>	0.0	7.0	−11.1
<i>syn-P/cis-S</i>	4.5	5.1	−14.9	<i>syn-P/trans-P</i>	2.3	13.5	−7.8
<i>syn-P/cis-P</i>	4.4	15.3	−5.5	<i>syn-P/trans-S</i>	2.5	5.4	−9.9

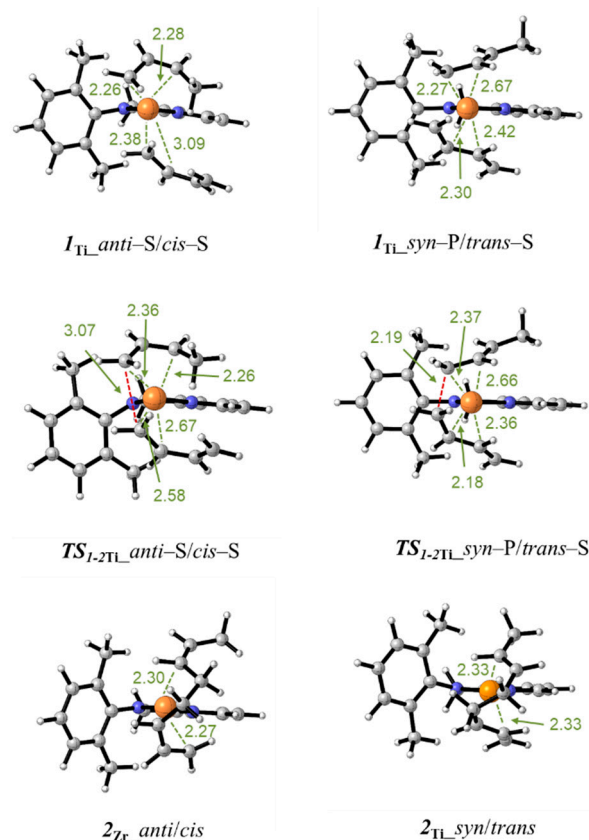


Figure 5. Minimum energy structures for the butadiene– π complex 1_{Ti} , the transition state TS_{1-2Ti} , and the insertion product 2_{Ti} . The isomers having the *anti*-butenyl group and the *cis*-coordinated butadiene (left column) and having the *syn*-butenyl group and the *trans*-coordinated butadiene (right column) are displayed. The distances are given in Angstrom.

The Gibbs free-energy change for the coordination of butadiene on the cation active species (ΔG_{coord}) is also affected by the steric crowding around the metal ion. As matter of fact, the average value of ΔG_{coord} for the titanium active species is -17.3 kcal/mol, whereas the average value of ΔG_{coord} for the zirconium active species is -21.1 kcal/mol. The less favored butadiene coordination on the titanium active species could be related to the lower polymerization activity of the titanium catalysts with respect to that observed for the zirconium analogues.

The butadiene insertion into the Ti–butenyl bond passes through the transition states TS_{1-Ti} whose Gibbs free energies are reported in Table 2. In Figure 5, the optimized structure of $TS_{1-2Ti_anti-S/cis-S}$ and $TS_{1-2Ti_syn-P/trans-S}$ are reported, and the distances of the forming C–C bond are 3.07 Å and 2.19 Å, respectively. Following the intrinsic reaction coordinate, the transition state structures lead to the products of the reaction 2_{Ti} . The reaction is exergonic for all the considered cases.

Also, in this case, to discuss the *cis/trans* selectivity, we exclusively focused on those isomers to which the lowest activation barriers correspond. The corresponding Gibbs free-energy profile is given in Figure 6. By the inspection of this graph, it appears that *path 1*, *path 2*, and *path 4* have very close activation barriers. This means that the η^3 -*anti*-isomer, through repeated *s-cis*-butadiene insertion, affords solely 1,4-*cis* repeating units, whereas the η^3 -*syn* isomer, through repeated *s-cis* and *s-trans*-butadiene insertion, affords 1,4-*cis* and 1,4-*trans* repeating units with equal rates. Accordingly, the generation of the *cis*-1,4-units is more probable than the generation of the 1,4-*trans* units. This agrees with the microstructure of the 1,4-polybutadiene obtained by using the titanium-based catalyst, which is predominantly 1,4-*cis* [30].

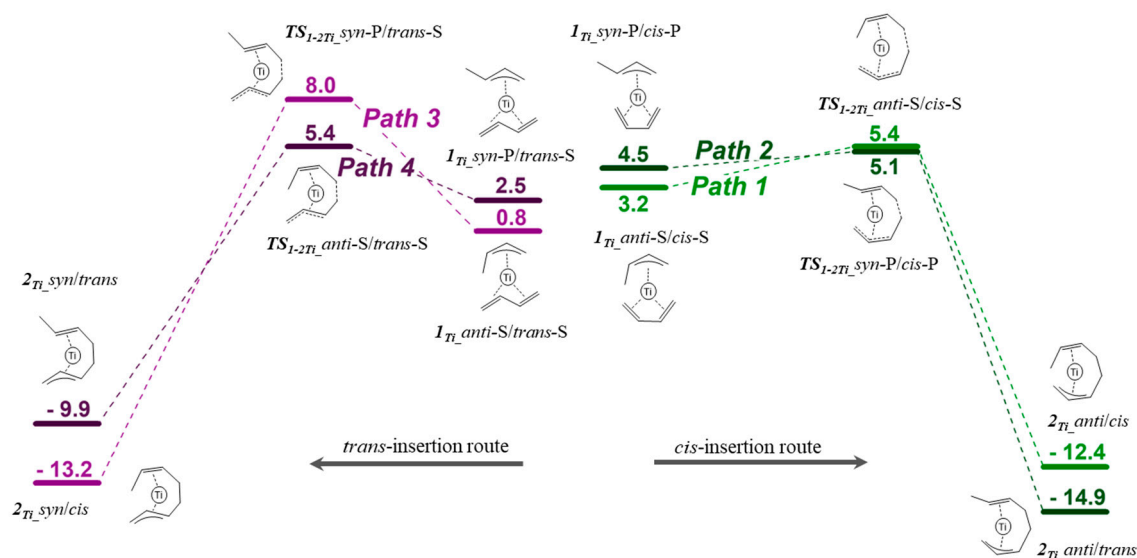


Figure 6. Gibbs free-energy profile for butadiene insertion in the Ti-butenyl bond.

Notwithstanding a deep analysis of the transition state structures for both zirconium and titanium catalytic systems, we did not succeed in correlating their energies with parameters such as bond distances or atom charges. In our opinion, the Gibbs free-energy profile and the competitiveness between the different reaction paths is the result of a delicate balance between the electronic and steric characteristics of the (anilidomethyl)pyridine ligand, the steric encumber in the first coordination sphere, and the properties of the metallic ion.

4. Conclusions

Impressed by the unique catalytic performance of the (anilidomethyl)pyridine group (IV) complexes in the polymerization of 1,3-butadiene, we conducted an extensive DFT investigation of the mechanism of stereoselective 1,4-butadiene insertion in the Mt-butenyl bond.

We started our investigation by probing the model for the active species. In a first instance, we considered the monovalent dialkyl cation that forms from the reaction of the precatalyst with the activating agent, in accordance with the expected active species involved in Ziegler–Natta polymerization. The results achieved are not in accordance with the experimental results. Thus, we moved to consider as active species the divalent monoalkyl cation resulting from the abstraction of two alkyl groups, having the following formula $(\text{NN})\text{MtR}(\text{CH}_2=\text{CHCH}=\text{CH}_2)^{2+}$. With this model, the results agree with the experimental data.

We investigated all the reaction paths involved in the insertion of butadiene into the Mt-butenyl bond. In the case of the zirconium catalytic system, the reaction paths leading to the 1,4-*cis* repeating unit resulted in being favorable with respect to those leading to the 1,4-*trans* repeating unit. The *syn-anti* isomerization, a process that could affect the stereoregularity of the polymer chain, resulted in being not competitive with respect to the propagation step. In the case of the titanium catalytic system, the computed reaction profile revealed that the paths for 1,4-*cis* or 1,4-*trans* enchainment occur with very similar activation energies thus resulting in being not competitive. The different reactivity of the two catalytic systems must be sought in the different dimensions of the metal atoms. In the case of titanium atoms, because of the smaller dimension, a greater repulsion is established among the polymer chain, the monomer, and the ancillary ligand. This in turn destabilizes the coordination adduct (as demonstrated by the lower free-energy change for the butadiene coordination) and alters the reaction profile rendering no paths competitive.

The results achieved herein show that the stereoselectivity of the 1,4-polymerization of butadiene with the (anilidomethyl)pyridine group IV catalysts is the result of a subtle balance between steric and electronic effects of the ancillary ligand and the choice of the metal center.

Supplementary Materials: The following supporting information can be downloaded at: <https://www.mdpi.com/article/10.3390/sym16010018/s1>. Cartesian coordinates and absolute energies (in a.u.) of all computed species.

Author Contributions: Conceptualization, S.M. and S.P.; validation, S.M. and S.P.; investigation, S.M.; writing—original draft preparation, S.M. and S.P.; writing—review and editing, S.M. and S.P.; funding acquisition, S.P. All authors have read and agreed to the published version of the manuscript.

Funding: This research received funding from Prin2020 (2020EZ8EPB).

Data Availability Statement: The data that support the findings of this study are available from the corresponding author upon reasonable request.

Acknowledgments: Financial support came from the “Ministero dell’Università e della Ricerca” (MUR) and is gratefully acknowledged.

Conflicts of Interest: The authors declare no conflicts of interest.

References

1. Kumar, A.; Mohanty, S.; Gupta, V.R. Butadiene Rubber: Synthesis, Microstructure, and Role of Catalysts. *Rubber Chem. Technol.* **2021**, *94*, 393–409. [[CrossRef](#)]
2. Porri, L.; Giarrusso, A. Conjugated Diene Polymerization. In *Comprehensive Polymer Science*; Eastmon, G.C., Ledwith, A., Russo, S., Sigwalt, P., Eds.; Elsevier: Oxford, UK, 1989; Volume 4, pp. 53–108.
3. Takeuchi, D. Stereoselective polymerization of conjugated dienes. In *Encyclopedia of Polymer Science and Technology*, 4th ed.; Mark, H.F., Ed.; Wiley: New York, NY, USA, 2014; Volume 13, pp. 126–150.
4. Ricci, G.; Leone, G. Polymerization of 1,3-butadiene with organometallic complexes-based catalysts. In *Applied Homogeneous Catalysis with Organometallic Compounds: A Comprehensive Handbook in Four Volumes*, 3rd ed.; Cornils, B., Hermann, W.A., Beller, M., Paciello, R., Eds.; Wiley-VCH Verlag GmbH: Weinheim, Germany, 2017; Volume 1, p. 251.
5. Ricci, G.; Pampaloni, G.; Sommazzi, A.; Masi, F. Dienes Polymerization: Where We Are and What Lies Ahead. *Macromolecules* **2021**, *54*, 5879–5914. [[CrossRef](#)]
6. Ricci, G.; Leone, G. Recent advances in the polymerization of butadiene over the last decade. *Polyolefins J.* **2014**, *1*, 43–60.
7. Pino, P.; Giannini, U.; Porri, L. Insertion Polymerization. In *Encyclopedia of Polymer Science and Engineering*, 2nd ed.; Mark, H.F., Bikales, N.M., Overberger, C.G., Menges, G., Eds.; Wiley: New York, NY, USA, 1987; Volume 8, pp. 147–220.
8. Porri, L.; Giarrusso, A.; Ricci, G. On the Mechanism of Formation of Isotactic and Syndiotactic Polydiolefins. *Macromol. Symp.* **2002**, *178*, 55–68. [[CrossRef](#)]
9. Porri, L.; Ricci, G.; Shubin, N. Polymerization of 1,3-dienes with neodymium catalysts. *Macromol. Symp.* **1998**, *128*, 53–61. [[CrossRef](#)]
10. Porri, L.; Giarrusso, A.; Ricci, G. Recent views on the mechanism of diolefin polymerization with transition metal initiator systems. *Prog. Polym. Sci.* **1991**, *16*, 405–441. [[CrossRef](#)]
11. Pragliola, S.; Botta, A.; Longo, P. Solvent effect in 1,3-butadiene polymerization by cyclopentadienyl titanium trichloride (CpTiCl₃)/methylaluminoxane (MAO) and pentamethylcyclopentadienyl titanium trichloride (Cp*TiCl₃)/MAO catalysts. *Eur. Polym. J.* **2019**, *111*, 20–27. [[CrossRef](#)]
12. Pragliola, S.; Costabile, C.; Venditto, V. Ethylene/1,3-butadiene cyclocopolymerization catalyzed by zirconocene systems. *Eur. Polym. J.* **2014**, *58*, 157–163. [[CrossRef](#)]
13. Nath, D.C.D.; Shiono, T.; Ikeda, T. Copolymerization of 1,3-butadiene and isoprene with cobalt dichloride/methylaluminoxane in the presence of triphenylphosphine. *J. Polym. Sci. A Polym. Chem.* **2002**, *40*, 3086–3092. [[CrossRef](#)]
14. Kaita, S.; Takeguchi, Y.; Hou, Z.; Nishiura, M.; Doi, Y.; Wakatsuki, Y. Pronounced Enhancement Brought in by Substituents on the Cyclopentadienyl Ligand: Catalyst System (C₅Me₄R)₂Sm(THF)_x/MMAO (R = Et, iPr, nBu, TMS; MMAO = Modified Methylaluminoxane) for 1,4-Cis Stereospecific Polymerization of 1,3-Butadiene in Cyclohexane Solvent. *Macromolecules* **2003**, *36*, 7923–7926.
15. Maiwald, S.; Sommer, C.; Müller, G.; Taube, R. Highly Active Single-Site Catalysts for the 1,4-cis Polymerization of Butadiene from Allylneodymium(III) Chlorides and Trialkylaluminiums—A Contribution to the Activation of Tris(allyl)neodymium(III) and the Further Elucidation of the Structure-Activity Relationship. *Macromol. Chem. Phys.* **2002**, *203*, 1029–1039.
16. Milione, S.; Cuomo, C.; Capacchione, C.; Zannoni, C.; Grassi, A.; Proto, A. Stereoselective Polymerization of Conjugated Dienes and Styrene—Butadiene Copolymerization Promoted by Octahedral Titanium Catalyst. *Macromolecules* **2007**, *40*, 5638–5643. [[CrossRef](#)]

17. Pires, N.M.T.; Ferreira, A.A.; de Lira, C.H.; Coutinho, P.L.A.; Nicolini, L.F.; Soares, B.G.; Coutinho, F.M.B. Performance Evaluation of High-cis 1,4-Polybutadienes. *J. Appl. Polym. Sci.* **2006**, *99*, 88–99. [[CrossRef](#)]
18. Pires, N.M.T.; Coutinho, F.M.B.; Costa, M.A.S. Synthesis and characterization of high cis-polybutadiene: Influence of monomer concentration and reaction temperature. *Eur. Polym. J.* **2004**, *40*, 2599–2603. [[CrossRef](#)]
19. Gargani, L.; Bruzzone, M. Fatigue Resistance of Polybutadienes and Effect of Microstructure. In *Advances in Elastomers and Rubber Elasticity*; Lal, J., Mark, J.E., Eds.; Springer US: Boston, MA, USA, 1986; pp. 233–251.
20. Ricci, G.; Sommazzi, A.; Masi, F.; Forni, A. Polymerization of 1,3-Butadiene with Catalysts Based on Cobalt Dichloride Complexes with Aminophosphines: Switching the Regioselectivity by Varying the MAO/Co Molar Ratio. *Chin. J. Polym. Sci.* **2023**, *in press*. [[CrossRef](#)]
21. Cass, P.; Pratt, K.; Mann, T.; Laslett, B.; Rizzardo, E.; Burford, R. Investigation of methylaluminumoxane as a cocatalyst for the polymerization of 1,3-butadiene to high cis-1,4-polybutadiene. *J. Polym. Sci. A Polym. Chem.* **1999**, *37*, 3277–3284. [[CrossRef](#)]
22. Endo, K.; Hatakeyama, N. Stereospecific and molecular weight-controlled polymerization of 1,3-butadiene with Co (acac) 3-MAO catalyst. *J. Polym. Sci. Part A Polym. Chem.* **2001**, *39*, 2793–2798. [[CrossRef](#)]
23. Sivaram, S.; Upadhyay, V.K. Synthesis of High-cis-Polybutadiene Using Cobalt (II)-2-Ethylhexoate Modified Triethylaluminum Catalyst. *J. Macromol. Sci. Pure Appl. Chem.* **1992**, *29*, 13–19. [[CrossRef](#)]
24. Wang, B.; Liu, H.; Tang, T.; Zhang, T. cis-1,4 Selective Coordination Polymerization of 1,3-Butadiene and Copolymerization with Polar 2-(4-Methoxyphenyl)-1,3-butadiene by Acenaphthene-Based α -Diimine Cobalt Complexes Featuring Intra-Ligand π - π Stacking Interactions. *Polymers* **2021**, *13*, 3329. [[CrossRef](#)]
25. Gong, D.; Jia, X.; Wang, B.; Zhang, X.; Jiang, L. Synthesis, characterization, and butadiene polymerization of iron(III), iron(II) and cobalt(II) chlorides bearing 2,6-bis(2-benzimidazolyl)pyridyl or 2,6-bis(pyrazol)pyridine ligand. *J. Organomet. Chem.* **2011**, *702*, 10–18. [[CrossRef](#)]
26. Liu, W.; Pan, W.; Wang, P.; Li, W.; Mu, J.; Mu, J.; Weng, G.; Jia, X.; Gong, D.; Huang, K.W. Synthesis of mixed-ligand cobalt complexes and their applications in high cis-1,4-selective butadiene polymerization. *Inorganica Chim. Acta* **2015**, *436*, 132–138. [[CrossRef](#)]
27. Gong, D.; Liu, W.; Pan, W.; Chen, T.; Jia, X.; Huang, K.W.; Zhang, X. Tunable regioselectivity in 1,3-butadiene polymerization by using 2,6-bis(dimethyl-2-oxazolin-2-yl)pyridine incorporated transition metal (Cr, Fe and Co) catalysts. *J. Mol. Catal. A Chem.* **2015**, *406*, 78–84. [[CrossRef](#)]
28. Liu, J.; Fan, X.; Min, X.; Zhu, X.; Zhao, N.; Wang, Z. Synthesis of high cis-1,4 polybutadiene with narrow molecular weight distribution via a neodymium-based binary catalyst. *RSC Adv.* **2018**, *8*, 21926–21932. [[CrossRef](#)] [[PubMed](#)]
29. Friebe, L.; Nuyken, O.; Obrecht, W. Ziegler/Natta Catalysts and their Application in Diene Polymerization. In *Neodymium Based Ziegler Catalysts—Fundamental Chemistry. Advances in Polymer Science*; Nuyken, O., Ed.; Springer: Berlin/Heidelberg, Germany, 2006; Volume 204, pp. 5–7.
30. Annunziata, L.; Pragliola, S.; Pappalardo, D.; Tedesco, C.; Pellicchia, C. New (Anilidomethyl)pyridine Titanium(IV) and Zirconium(IV) Catalyst Precursors for the Highly Chemo- and Stereoselective cis-1,4-Polymerization of 1,3-Butadiene. *Macromolecules* **2011**, *44*, 1934–1941. [[CrossRef](#)]
31. Frisch, M.J.; Trucks, G.W.; Schlegel, H.B.; Scuseria, G.E.; Robb, M.A.; Cheeseman, J.R.; Scalmani, G.; Barone, V.; Petersson, G.A.; Nakatsuji, H.; et al. (Eds.) *Gaussian 16*, Revision C.01; Gaussian, Inc.: Wallingford, CT, USA, 2016.
32. Becke, A. Density-functional exchange-energy approximation with correct asymptotic behavior. *Phys. Rev. A* **1988**, *38*, 3098–3100. [[CrossRef](#)] [[PubMed](#)]
33. Perdew, J.P. Density-functional approximation for the correlation energy of the inhomogeneous electron gas. *Phys. Rev. B* **1986**, *33*, 8822–8824. [[CrossRef](#)] [[PubMed](#)]
34. Schäfer, A.; Huber, C.; Ahlrichs, R. Fully optimized contracted Gaussian basis sets of triple zeta valence quality for atoms Li to Kr. *J. Chem. Phys.* **1994**, *100*, 5829. [[CrossRef](#)]
35. Weigend, F.; Ahlrichs, R. Balanced basis sets of split valence, triple zeta valence and quadruple zeta valence quality for H to Rn: Design and assessment of accuracy. *Phys. Chem. Chem. Phys.* **2005**, *7*, 3297–3305. [[CrossRef](#)]
36. Zhao, Y.; Truhlar, D.G. The M06 suite of density functionals for main group thermochemistry, thermochemical kinetics, noncovalent interactions, excited states, and transition elements: Two new functionals and systematic testing of four M06-class functionals and 12 other functionals. *Theor. Chem. Acc.* **2008**, *120*, 215–241.
37. Falivene, L.; Cao, Z.; Petta, A.; Serra, L.; Poater, A.; Oliva, R.; Scarano, V.; Cavallo, L. Towards the online computer-aided design of catalytic pockets. *Nat. Chem.* **2019**, *11*, 872–879. [[CrossRef](#)]
38. Taube, R.; Schmidt, U.; Gehrke, J.-P.; Böhme, P.; Langlotz, J.; Wache, S. New mechanistic aspects and structure activity relationships in the allyl nickel complex catalysed butadiene polymerization. *Makromol. Chem. Makromol. Symp.* **1993**, *66*, 245–260. [[CrossRef](#)]
39. Taube, R.; Windisch, H.; Maiwald, S. The catalysis of the stereospecific butadiene polymerization by allyl nickel and allyl lanthanide complexes—A mechanistic comparison. *Macromol. Symp.* **1995**, *89*, 393–409. [[CrossRef](#)]
40. Tobisch, S.; Bögel, H.; Taube, R. Mechanistic studies of the 1,4-polymerization of butadiene according to the π -allyl-insertion mechanism. 2. Density functional study of the C-C bond formation reaction in cationic and neutral (η^3 -crotyl)(η^2 -/ η^4 -butadiene)nickel(II) complexes $[\text{Ni}(\text{C}_4\text{H}_7)(\text{C}_4\text{H}_6)]^+$, $[\text{Ni}(\text{C}_4\text{H}_7)]$. *Organometallics* **1996**, *15*, 3563–3571. [[CrossRef](#)]
41. Taube, R.; Sylvester, G. *Applied Homogeneous Catalysis with Organometallic Complexes*; Cornils, B., Herrmann, W.A., Eds.; VCH: Weinheim, Germany, 1996; pp. 280–317.

42. Peluso, A.; Improta, R.; Zambelli, A. Mechanism of Isoprene and Butadiene Polymerization in the Presence of CpTiCl₃–MAO Initiator: A Theoretical Study. *Macromolecules* **1997**, *30*, 2219–2227. [[CrossRef](#)]
43. Guerra, G.; Cavallo, L.; Corradini, P.; Fusco, R. Molecular mechanics and stereospecificity in Ziegler-Natta 1,2 and cis-1,4 polymerizations of conjugated dienes. *Macromolecules* **1997**, *30*, 677–684. [[CrossRef](#)]
44. Tobisch, S.; Taube, R. Mechanistic studies of the 1,4-polymerization of butadiene according to the π -allyl-insertion mechanism. 3. Density functional study of the C-C bond formation reaction in cationic “ligand-free” (η^3 : η^2 -heptadienyl) (η^2 -/ η^4 -butadiene)nickel(II) complexes [Ni(C₇H₁₁)(C₄H₆)]⁺. *Organometallics* **1999**, *18*, 5204–5218.
45. Costabile, C.; Milano, G.; Cavallo, L.; Guerra, G. Stereoselectivity and Chemoselectivity in Ziegler-Natta Polymerizations of Conjugated Dienes. 1. Monomers with Low-Energy s-Cis h⁴ Coordination. *Macromolecules* **2001**, *34*, 7952–7960. [[CrossRef](#)]
46. Taube, R.; Sylvester, G. Stereospecific polymerization of butadiene or isoprene. In *Applied Homogeneous Catalysis with Organometallic Compounds*, 2nd ed.; Cornils, B., Herrmann, W.A., Eds.; Wiley-VCH Verlag GmbH: Weinheim, Germany, 2002; Volume 1, pp. 285–315.
47. Tobisch, S. Reaction Mechanism in the Stereospecific 1,4-Polymerization of Butadiene with Ziegler-Natta Type Catalysts of Early Transition Metals: Comprehensive Density Functional Investigation for the Cationic [Ti^{III}Cp(polybutadienyl)(butadiene)]⁺ Active catalyst. *Organometallics* **2003**, *22*, 2729–2740. [[CrossRef](#)]
48. Tobisch, S. The stereospecific polymerization of 1,3-butadiene mediated by early and late transition-metal catalysts. Towards a deeper understanding of the catalytic structure–reactivity relationships from computational-mechanistic studies. *J. Mol. Struct. Theochem* **2006**, *771*, 171–179. [[CrossRef](#)]

Disclaimer/Publisher’s Note: The statements, opinions and data contained in all publications are solely those of the individual author(s) and contributor(s) and not of MDPI and/or the editor(s). MDPI and/or the editor(s) disclaim responsibility for any injury to people or property resulting from any ideas, methods, instructions or products referred to in the content.